Nonlinear optimisation method for image segmentation and noise reduction using geometrical intrinsic properties

S. Mahmoodi [a,*], B.S. Sharif [b]

[a] *Psychology Department, School of Biology, Henry Wellcome Building, Newcastle University, Newcastle upon Tyne, NE2 4HH*
[b] *School of Electrical, Electronic and Computer Engineering, Merz Court, Newcastle University, Newcastle upon Tyne, NE1 7RU, UK*

Abstract

This paper considers the optimisation of a nonlinear functional for image segmentation and noise reduction. Equations optimising this functional are derived and employed to detect edges using geometrical intrinsic properties such as metric and Riemann curvature tensor of a smooth differentiable surface approximating the original image. Images are then smoothed using a Helmholtz type partial differential equation. The proposed approach is shown to be very efficient and robust in the presence of noise, and the reported results demonstrate better performance than the conventional derivative based edge detectors.
© 2005 Elsevier B.V. All rights reserved.

1. Introduction

The methods of nonlinear energy optimisation for image segmentation and smoothing have recently received much attention in the literature (see e.g. [1–7,17–23]). 'Inverse problem' as a restoration method for signals and images was initially introduced by Tikhonov et al. [21]. This approach was then modified by Rudin et al. [22] to introduce the total variation method. Nonlinear optimisation based on the concept of bounded variation was later employed in the literature (see e.g. [23]). On the other hand, a segmentation algorithm known as 'snake' that uses a linear functional was first introduced by Kass et al. [1]. This was further developed as the Geodesic active contours model and the level-set method (e.g. See [8,15,16]). Mumford et al. [2–4] introduced a nonlinear functional to simultaneously segment and smooth images. This functional was further implemented using contour evolution approaches [5–7,17–20] based on the level set method [8]. A nonlinear functional was also proposed by Mahmoodi et al. [24,25] for signal segmentation and smoothing. This functional includes two terms (fidelity and smoothing terms) of the Mumford–Shah functional. However,

since the notion of contours is not defined in signal processing context, the third term (contour length minimisation) is not included. This functional is investigated for continuous and discrete signals and a general iterative algorithm based on the optimised equations is proposed in [24]. The geometric properties of the smoothed signal are also used in another algorithm proposed in [25] to segment and smooth a noisy signal. In this paper, the 2D version of the functional investigated in [24,25] is considered and equations optimising the functional are then derived. An approach based on geometrical intrinsic (GI) properties of a differentiable surface approximating the original image is then proposed to implement this functional. This approach can be considered as the generalisation of the geometrical algorithm employed in [25] for 2D images. Therefore, the theory of surfaces is exploited in this paper to propose an algorithm for image segmentation.

The structure of the paper is as follows. In Section 2, the theoretical formulas are derived by optimising a nonlinear functional. The implementation method is outlined in Section 3, and results are presented in Section 4. Finally, conclusions are drawn in Section 5.

2. Energy optimisation

Image $I(x,y)$ is considered as a piecewise continuous function with contours Γ_i representing discontinuities. The smoothed functions $f_i(x,y)$ of class C^n $n \geq 2$ composing

---

* Corresponding author.
E-mail address: sasan.mahmoodi@ncl.ac.uk (S. Mahmoodi).

piecewise smoothed image $f(x,y)$ are considered in an open set such as $S_i(x,y)$ which does not contain any discontinuity.

A functional is, therefore, defined to find the most optimised image $f(x,y)$ and $S_i(x,y)$ for every R_i so that, in region R_i, $f(x,y)$ approximates $I(x,y)$ as closely as possible and $f(x,y)$ is smoothed depending on μ; and smoothing is avoided over discontinuities

$$E(f,\Gamma) = \frac{1}{2}\sum_i \iint_{R_i-\Gamma_i} [(f_i(x,y)-I(x,y))^2 + \mu(\nabla f_i)^2]S_i(x,y)\mathrm{d}x\,\mathrm{d}y \tag{1}$$

where $E(f,\Gamma)$ is the functional to be optimised, $S_i(x,y)$ is an open connected [11,12] set R_i in which $I(x,y)$ has no discontinuities, i.e. Γ_i represents boundary of $S_i(x,y)$, and $\Gamma=\{\Gamma_i\}$. $S_i(x,y)$ can also be defined as

$$S_i(x,y) = \begin{cases} 1 & x,y \in R_i \\ 0 & x,y \notin R_i \end{cases}$$

In computer vision terms, $S_i(x,y)$ is the segmented image and $f_i(x,y)$ is the smoothed image.

Functional (1) is for the special case where $R_i \cap R_j = \varnothing$ for $i \neq j$, so that R_i and R_j are represented by $S_i(x,y)$ and $S_j(x,y)$. In this case, Γ_i is considered a closed curve. However, more generally, where Γ_i is not a closed curve, functional (1) can be written as

$$E(f,\Gamma) = \frac{1}{2}\sum_i \iint_{R_i-\Gamma_i} [(f_i(x,y)-I(x,y))^2 + \mu(\nabla f_i)^2]\mathrm{d}x\,\mathrm{d}y. \tag{2}$$

The objective in this paper is to find $f_i(x,y)$s and Γ_is that minimise functional (1) and (2). In this functional, minimisation of contour length is not required, which has two advantages; First, this functional leads to less numerical computations than the Mumford–Shah functional with equivalent results. Second, implementation complexities are less and therefore noniterative methods can be employed.

We start from functional (1) to establish a mathematical framework to find $f_i(x,y)$ and $S_i(x,y)$ using variational methods [9,10].

If we assume that δf_i is of the same class as f_i and f_i is varied by δf_i while $S_i(x,y)$ remains unchanged. By assuming a fixed function for $S_i(x,y)$, functional (1) can be considered convex (e.g. see chapter 3 in [9] pp. 39–44). The variations in functional (1), $\delta E = \delta E_i$ is calculated as

$$\delta E_i = E_i(f_i + \delta f_i) - E_i(f_i)$$

$$\begin{aligned}\delta E_i = \frac{1}{2}\iint &\left[\mu\left(\frac{\partial(f_i+m\delta f_i)}{\partial x}\right)^2 + \mu\left(\frac{\partial(f_i+m\delta f_i)}{\partial y}\right)^2 \right. \\ &\left. + (f_i+m\delta f_i-I)^2\right]S_i(x,y)\mathrm{d}x\mathrm{d}y \\ -\frac{1}{2}\iint &\left[\mu\left(\frac{\partial f_i}{\partial x}\right)^2 + \mu\left(\frac{\partial f_i}{\partial y}\right)^2 + (f_i-I)^2\right]S_i(x,y)\mathrm{d}x\,\mathrm{d}y\end{aligned}$$

The above equation can be rewritten as

$$\begin{aligned}\delta E = m\iint &\left[\mu\left(\frac{\partial f_i}{\partial x}\right)\left(\frac{\partial \delta f_i}{\partial x}\right) + \mu\left(\frac{\partial f_i}{\partial y}\right)\left(\frac{\partial \delta f_i}{\partial y}\right) + \delta f_i(f_i-I)\right. \\ &\left. +m\mu\left(\frac{\partial f_i}{\partial x}\right)^2 + m\mu\left(\frac{\partial f_i}{\partial y}\right)^2 + m\delta f_i^2\right]S_i(x,y)\mathrm{d}x\,\mathrm{d}y\end{aligned}$$

Therefore:

$$\begin{aligned}\frac{\delta E_i}{\delta f_i} &= \lim_{m\to 0}\left(\frac{\delta E_i}{m}\right) \\ &= \iint_{R_i-\Gamma_i}\left[\mu\left(\frac{\partial f_i}{\partial x}\right)\left(\frac{\partial \delta f_i}{\partial x}\right) + \mu\left(\frac{\partial f_i}{\partial y}\right)\left(\frac{\partial \delta f_i}{\partial y}\right) + \delta f_i(f_i-I)\right]\mathrm{d}x\,\mathrm{d}y\end{aligned}$$

By integrating in part and considering that the line integral on the closed contour Γ_i should be in one direction either clockwise or counter clockwise over the contour, then we obtain

$$\frac{\delta E_i}{\delta f_i} = \mu\int_{\Gamma_i}\delta f_i(\vec{\nabla}f_i.\vec{n})\mathrm{d}s - \iint_{R_i-\Gamma_i}\delta f_i(-\mu\nabla^2 f_i + (f_i-I))\mathrm{d}x\,\mathrm{d}y$$

or

$$\frac{\delta E_i}{\delta f_i} = \mu\int_{\Gamma_i}\delta f_i\left(\frac{\partial f_i}{\partial n}\right)\mathrm{d}s - \iint_{R_i-\Gamma_i}\delta f_i(-\mu\nabla^2 f_i + (f_i-I))\mathrm{d}x\,\mathrm{d}y \tag{3}$$

where $\vec{n}$ is the unit normal vector to the contour path Γ_i, $\mathrm{d}s = \sqrt{\mathrm{d}x^2 + \mathrm{d}y^2}$ is the element of arc length, $\vec{\nabla}$ is gradient operator and ∇^2 is Laplacian operator. In order to find the optimised solution, Eq. (3) is set to zero, since $\delta f_i \neq 0$ in $R_i-\Gamma_i$, then

$$\mu\nabla^2 f_i = f_i - I \quad \text{in } R_i - \Gamma_i \tag{4}$$

Eq. (4) is of Helmholtz type equation. Since the boundary condition is not known on contour Γ_i, the problem is treated as a free boundary condition (chapter 7 in [9] pp. 98–107). In this context, the first term is set to zero to obtain the boundary condition on contour Γ_i

$$\frac{\partial f_i}{\partial n} = 0 \quad \text{in } \Gamma_i \tag{5}$$

Let us now vary Γ_i in a small neighbourhood of an arbitrary point P on contour Γ_i between two regions S_i and S_{i+1} (as shown in Fig. 1) and calculate variations of functional (1). Obviously, f_i is varied in a neighbourhood N of P and these variations in f_i are considered in the calculations of the functional variations.
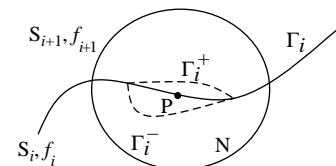

Fig. 1. Variations of contour Γ_i in a small neighbourhood of a point P.

If Γ_i is varied to Γ_i^+ and Γ_i^- in the neighbourhood N of point P shown in Fig. 1, the variations of functional (1) are calculated as

$$E^+(f^+, \Gamma^+) = \frac{1}{2} \sum_i \iint\limits_{R_i^+ - \Gamma_i^+} [(f_i^+(x,y) - I(x,y))^2$$

$$+ \mu(\nabla f_i^+)^2] S_i^+(x,y) \mathrm{d}x\,\mathrm{d}y$$

$$E^-(f^-, \Gamma^-) = \frac{1}{2} \sum_i \iint\limits_{R_i^- - \Gamma_i^-} [(f_i^-(x,y) - I(x,y))^2$$

$$+ \mu(\nabla f_i^-)^2] S_i^-(x,y) \mathrm{d}x\,\mathrm{d}y$$

$$\delta E = E^+ - E^- = \frac{1}{2} \sum_{j=i}^{i+1} \iint\limits_{R_j^+ - \Gamma_j^+} [(f_j^+(x,y) - I(x,y))^2$$

$$+ \mu(\nabla f_j^+)^2] S_j^+(x,y)\mathrm{d}x\mathrm{d}y - \frac{1}{2}$$

$$\times \sum_{j=i}^{i+1} \iint\limits_{R_j^- - \Gamma_j^-} [(f_j^-(x,y) - I(x,y))^2$$

$$+ \mu(\nabla f_j^-)^2] S_j^-(x,y)\mathrm{d}x\mathrm{d}y$$

or

$$\delta E = \frac{1}{2} \iint\limits_{R_i^+ \cup R_{i+1}^+ - \Gamma_i^+} [(f^+(x,y) - I(x,y))^2$$

$$+ \mu(\nabla f^+)^2] S^+(x,y)\mathrm{d}x\,\mathrm{d}y - \frac{1}{2}$$

$$\times \iint\limits_{R_i^- \cup R_{i+1}^- - \Gamma_i^-} [(f^-(x,y) - I(x,y))^2 + \mu(\nabla f^-)^2] S^-(x,y)\mathrm{d}x\,\mathrm{d}y$$

$$\delta E = \frac{1}{2} \iint\limits_N [(f^+(x,y) - I(x,y))^2 + \mu(\nabla f^+)^2$$

$$- (f^-(x,y) - I(x,y))^2 - \mu(\nabla f^-)^2]\mathrm{d}x\,\mathrm{d}y \qquad (6)$$

where f^+ and f^- are defined as:

$$f^+ = \begin{cases} f_i^+ & (x,y) \in N \& (x,y) \in R_i \\ f_{i+1}^+ & (x,y) \in N \& (x,y) \in R_{i+1} \\ \text{unchanged} & (x,y) \notin N \end{cases}$$

$$f^- = \begin{cases} f_i^- & (x,y) \in N \& (x,y) \in R_i \\ f_{i+1}^- & (x,y) \in N \& (x,y) \in R_{i+1} \\ \text{unchanged} & (x,y) \notin N \end{cases}$$

If we represent contour Γ_i as a natural representation $\mathbf{\Gamma}_i = \mathbf{\Gamma}_i(x(s), y(s))$, then Γ_i^+ can be represented as either

$\Gamma_i^+ = \mathbf{\Gamma}_i^+(x(s), y(s) + m\delta y(s)/2)$ or $\mathbf{\Gamma}_i^+ = \mathbf{\Gamma}_i^+(x(s) + m\delta x(s)/2, y(s))$. Γ_i^- can be represented by the same form as Γ_i^+. Using the first form for Γ_i^+ and Γ_i^-, Eq. (6) can, therefore, be rewritten as

$$\delta E = \frac{1}{2} \int \int\limits_{y - m\delta y/2}^{y + m\delta y/2} [(f^+(x,y) - I(x,y))^2 + \mu(\nabla f^+)^2$$

$$- (f^-(x,y) - I(x,y))^2 - \mu(\nabla f^-)^2]\mathrm{d}y\,\mathrm{d}x$$

or

$$\frac{\delta E}{\delta \Gamma_i} = \lim_{m \to 0} \frac{\delta E}{m} = \frac{1}{2} \int\limits_N [(f^+(x,y) - I(x,y))^2 + \mu(\nabla f^+)^2$$

$$- (f^-(x,y) - I(x,y))^2 - \mu(\nabla f^-)^2]\delta y\,\mathrm{d}x$$

In order to find the condition under which functional (1) is optimised with respect to the variations of Γ_i, the above equation is set to 0, i.e.

$$\int\limits_N [(f^+(x,y) - I(x,y))^2 + \mu(\nabla f^+)^2 - (f^-(x,y) - I(x,y))^2$$

$$- \mu(\nabla f^-)^2]\delta y\,\mathrm{d}x = 0$$

Since δy is not zero in the neighbourhood N, we obtain

$$(f^+(x,y) - I(x,y))^2 + \mu(\nabla f^+)^2 - (f^-(x,y) - I(x,y))^2$$
$$- \mu(\nabla f^-)^2 = 0 \qquad (7)$$

The geometrical concept of Eq. (7) is that the contour Γ_i is the intersection between two surfaces $(f^+(x,y) - I(x,y))^2 + \mu(\nabla f^+)^2$ and $(f^-(x,y) - I(x,y))^2 + \mu(\nabla f^-)^2$. Although the two surfaces have common points in continuous regions, however, in the neighbourhood of discontinuity, they only intersect at the contour Γ_i. Eqs. (4), (5) and (7) can also be extended to obtain optimised solutions for the case where Γ_i is any nonclosed curve, i.e. they optimise functional (2) as well.

3. Implementation method

Original image can be approximated by minimising linear functional (8) to obtain a smooth and differentiable surface $f(x,y)$:

$$E(f) = \frac{1}{2} \sum \iint\limits_R [(f(x,y) - I(x,y))^2 + \mu(\nabla f)^2]\mathrm{d}x\,\mathrm{d}y \qquad (8)$$

By optimising functional (8) using Euler–Lagrange equation, the following differential equation is obtained:

$$\mu \nabla^2 f = f - I \qquad (9)$$

The solution for the above partial differential equation can be considered as a smooth differentiable Monge patch represented as [11,12]:

$$\mathbf{S}(x^1, x^2) = x^1 \mathbf{e}_1 + x^2 \mathbf{e}_2 + f(x^1, x^2)\mathbf{e}_3 \qquad (10)$$

where (x^1, x^2) are coordinates corresponding to (x,y) and $\mathbf{e}_1$, $\mathbf{e}_2$, $\mathbf{e}_3$ are unit vectors $\mathbf{i}$, $\mathbf{j}$ and $\mathbf{k}$ in a Euclidean manifold of three dimensions. This surface can be described using Gauss differential equations in tensor notation as (chapter 10 in [11] pp. 201–215, chapter 4 in [12] pp. 231–237)

$$\partial_i \partial_j \mathbf{S} = \Gamma_{ij}^k \partial_k \mathbf{S} + b_{ij}\mathbf{N} \quad (i,j,k = 1,2) \tag{11}$$

where Γ_{ij}^k are Christoffel symbols of the second kind, b_{ij} are components of a covariant tensor field of rank two representing the second fundamental coefficients of surfaces and $\mathbf{N}$ is the unit normal vector to the surface. In Eq. (11), Einstein summation convention is employed (chapter 1 in [26]). Christoffel symbols are computed by the first fundamental coefficients or metric tensors represented by g_{ij} and their derivatives [11,12]. Therefore, according to Eq. (11), a surface can be uniquely determined by using its metric tensors and tensors representing its second fundamental coefficients (chapter 10 in [11] pp. 203–208). In this paper, an algorithm is proposed to detect edges represented as discontinuities of the original image $I(x,y)$, by considering the smooth surface calculated from Eq. (9).

Normal curvature in any point on a smooth surface with metric tensors g_{ij} and the second fundamental coefficients tensors b_{ij} is calculated as (chapter 9 in [11] pp. 179–181)

$$\kappa_n = \frac{b_{11}(dx^1)^2 + 2b_{12}dx^1 dx^2 + b_{22}(dx^2)^2}{g_{11}(dx^1)^2 + 2g_{12}dx^1 dx^2 + g_{22}(dx^2)^2} \tag{12}$$

where $dx^1 : dx^2$ is the orientation along which normal curvature is computed. On the smooth surface obtained by solving Eq. (9), normal curvature along an orientation perpendicular to the tangent of the contour representing discontinuity is zero. This can further be investigated in Eq. (12), by substituting $X = dx^1/dx^2$

$$\kappa_n = \frac{b_{11}X^2 + 2b_{12}X + b_{22}}{g_{11}X^2 + 2g_{12}X + g_{22}}$$

Zero value for normal curvature requires that

$$b_{11}X^2 + 2b_{12}X + b_{22} = 0 \tag{13}$$

In general, if $b_{ij} \neq 0$, there is only one orientation along which normal curvature is zero. This is the orientation normal to the contour. Therefore, Eq. (13) should have only one single real root with multiplicity two. This is achieved when the discriminant of Eq. (13) is zero, i.e.:

$$b_{12}^2 - b_{11}b_{22} = 0 \tag{14}$$

Quantity $b_{12}^2 - b_{11}b_{22}$ is a GI property of surfaces and is known as covariant Riemann tensor curvature. Orientation, along which normal curvature is zero, is the single real root of Eq. (13). This orientation is normal to edge path and calculated as:

$$X = -\frac{b_{12}}{b_{11}} \tag{15}$$

Eq. (15) could be used to apply boundary condition of Eq. (5) on edge paths and contours. The condition indicated in

Eq. (14) can also be obtained by considering zero value for one of the principle curvatures. This implies that the Gaussian curvature of the surface in the point in question should be zero and hence condition (14) is satisfied. Such points on the surface are known as parabolic points (chapter 9 in [11] pp. 175–187). The other principle curvature then determines the curvature of the contour.

Area element on a smooth surface is another GI property that is used to detect discontinuities in the original image. On a smooth surface of an image, discontinuities correspond to regions with maximum area element on the smooth surface. For a surface with metric tensor g_{ij}, area element on the surface is calculated as the discriminant of metric tensor

$$g = \frac{|\Delta \mathbf{S}|}{\Delta x^1 \Delta x^2} = \sqrt{g_{11}g_{22} - g_{12}^2} \tag{16}$$

Therefore, if we start from a smooth surface obtained from Eq. (9), the edges correspond to points where Riemann tensor curvature is zero and Eq. (16) is maximised. Riemann curvature tensor and area variation calculated by Eq. (16) are initially computed for the whole image. Maximum values for this quantity in regions of zero Riemann curvature correspond to edges in the image. Since discriminant of metric tensor is definite positive, its minimum value is one corresponding to points with no variations. Therefore, a point is considered edge point if its tensor curvature is zero, its area is a local maximum and this maximum value is greater than a threshold.

Having segmented the image, Eq. (4) with the boundary condition (5) is applied to reduce the noise from the original image. To implement this noise reduction process, we start from the segmented image. For every pixel located at i, j a 3×3 window whose centre is at i, j is considered. If there is no segmented pixel in this window, the value of pixel at i, j for the smoothed image is calculated using the discrete version of Eq. (4) estimated by finite difference method [14], i.e.

$$f(i,j) = \frac{\mu(f(i-1,j) + f(i+1,j) + f(i,j-1) + f(i,j+1))}{4\mu + 1}$$

$$+ \frac{I(i,j)}{4\mu + 1}$$

where $I(i,j)$ is the pixel value at i, j from the noisy image. However, if any of the pixels' locations at $(i-1,j)$, $(i,j-1)$, $(i+1,j)$, and $(i,j+1)$ are segmented, then the second derivative in Eq. (4) is estimated using the pixel values of the unsegmented pixels. For instance if the pixel at location $(i-1,j)$ is segmented, the pixel value of the smoothed image at location (i,j) is estimated as:

$$f(i,j) = \frac{\mu(f(i+1,j) + f(i,j-1) + f(i,j+1))}{3\mu + 1} + \frac{I(i,j)}{3\mu + 1}$$

However, if the pixel in location (i,j) is a segmented pixel, then boundary condition of Eq. (5) is applied to determine the pixel value of the smoothed image at location (i,j). For example, if the orientation of the contour passing through pixel (i,j) is horizontal (parallel to x-axis or the axis representing columns j) then either $f(i-1,j)$ or $f(i+1,j)$ can be chosen

depending on how close their pixel value is to $f(i,j)$. This method guarantees sharp edges in a neighbourhood of an edge path in the smoothed image. Calculation methods of parameters b_{ij}, g_{ij} and curvature tensor are presented in the Appendix.

4. Results

A noiseless synthetic image shown in Fig. 2(a), is contaminated with Gaussian noise to obtain a noisy image shown in Fig. 2(b) with SNR=4.2. The GI based algorithm described in Section 3 is applied to this noisy image. The segmented images are depicted in Fig. 2(c)-(e) and smoothed images obtained by applying Eq. (4) with boundary condition (5) is shown in Fig. 2(f)-(h). μ=0.1, 5, and 50 are used to smooth the noisy image. As shown from this figure, segmentation is unaffected for values of μ higher than a threshold depending on the SNR of the image.

Values of μ lower than this threshold result in partial or under segmentation, as shown in Fig. 2(c). This is due to the fact that with low values of μ, edges as well as some portions of noise in the image have the required geometrical properties for segmentation. However, by increasing μ, the required geometrical properties for edges remain unchanged, while noise is heavily smoothed which results in changes in their geometrical properties. This also suggests that small objects of the order of few pixels such as noise might not be detected when a high value of μ is chosen. It is, therefore, concluded that higher values for μ should be chosen when the amount of noise in an image is increased. A smoother image is also obtained when higher values of μ are chosen. This is demonstrated in Fig. 2(f)–(h).

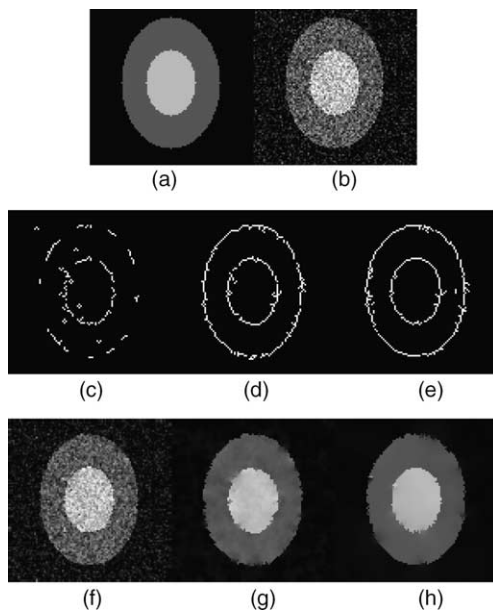

Fig. 2. Original noiseless image (a) noisy image contaminated with Gaussian noise with SNR=4.2 (b) Segmented image using the GI algorithm described in Section 3 using μ=0.1 (c), μ=5 (d) and μ=50 (e) smoothed image with μ=0.1 (f), μ=5 (g) and μ=50 (h).
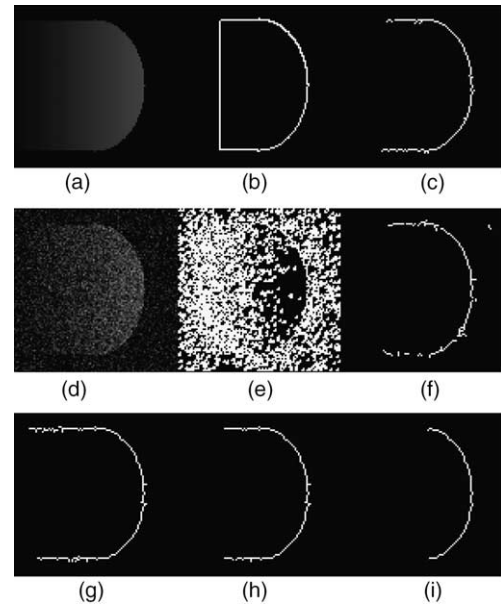

Fig. 3. Original noiseless image characterised with a nonclosed contour (a) contour detection of the noiseless image using the iterative method proposed in Ref. [6] implementing Mumford–Shah functional, (b) contour detection using the GI algorithm, (c) noisy image with SNR=1, (d) contour detection using the iterative method proposed in Ref. [6], (e) contour detection using the GI algorithm, (f) contour detection of the original noiseless image using a threshold set to, (g) 0.15, (h), 0.35, (i) 0.65.

Contour of objects in images can also be open. Fig. 3(a) shows an image containing an object with a nonclosed contour. Gaussian noise is added to this image to obtain the image of Fig. 3(d) with SNR=1. The edge detected images using an iterative method implementing Mumford–Shah functional [6,17–20] and GI method are depicted in Fig. 3(b) and (c), respectively.

As shown in Fig. 3(b), the detected contour using this iterative algorithm is a closed contour, i.e. one part of the resulting contour does not actually exist as an edge in the original image. This is basically an artefact of the iterative method. This problem is resolved in the GI algorithm as seen in Fig. 3(c). The iterative method proposed in [6,17–20] and GI algorithm is applied to the noisy image of Fig. 3(d). While the GI algorithm successfully segments the image as depicted in Fig. 3(f), the iterative method which is operational for a favourable SNR, fails to segment the image as demonstrated in Fig. 3(e). The GI algorithm with different threshold values is applied to the noiseless image of Fig. 3(a), and the results are shown in Fig. 3(g)–(i).

At this stage, it is interesting to investigate the noise sensitivity of our algorithm and compare this method to the derivative of Gaussian (*DroG*) edge detection algorithm [13]. An original noiseless image is contaminated with Gaussian noise with different variances to obtain noisy images with SNR=0.5, 0.25, 0.03 as depicted in Fig. 4. The proposed GI algorithm in this paper is applied to the noisy images to obtain the segmented images. Noise reduction is also achieved by applying Eq. (4) with boundary condition (5) as shown in Fig. (4). Edge detection algorithm based on *DroG* is finally
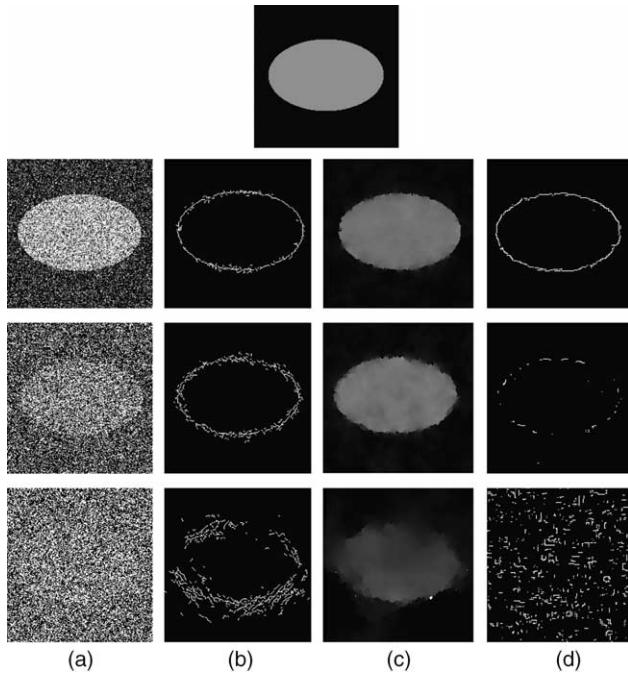
Fig. 4. Original noiseless image (top) noisy images contaminated with Gaussian noise with SNR=0.5, 0.25 and 0.03 (column a) segmented images using the proposed GI algorithm (column b) smoothed images using the proposed algorithm (column c) segmented images using *DroG* edge detector with window size 9×9, and empirically optimised standard deviations and threshold values (column d).

applied to the noisy images for comparison. It should be noted that in both cases, empirically optimised threshold values were used for fair comparison. The window size for this *DroG* algorithm is chosen as 9×9 and empirically optimal standard deviations of the Gaussian function is chosen. As can be seen from Fig. (4), *DroG* operator starts failing for the noisy image with SNR=0.25. This failure is more clear for the noisy image with SNR=0.03. A better performance of GI algorithm than that of the *DroG* operator is clearly observed from this figure. This point is further investigated in Fig. 5. It should be noted that noise reduction is considered as a by-product of our method. This bonus however is absent in the *DroG* edge detector.

A further comparison has been made between the *DroG* edge detector and GI algorithm as depicted in Fig. 5. A noiseless image of Fig. 5(a) is contaminated with Gaussian noise to obtain a noisy image with SNR=0.28 as shown in Fig. 5(b). This image is segmented using the *DroG* edge
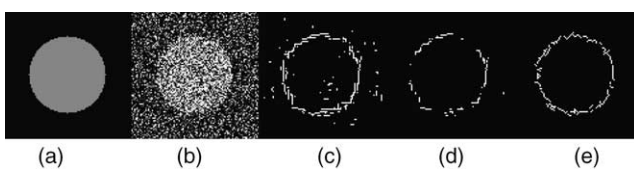

Fig. 5. Original noiseless image (a), noisy image with SNR=0.28 (b) segmented image using *DroG* operator with different threshold values (c) and (d) segmented image using GI algorithm with $\mu = 100$ (e).
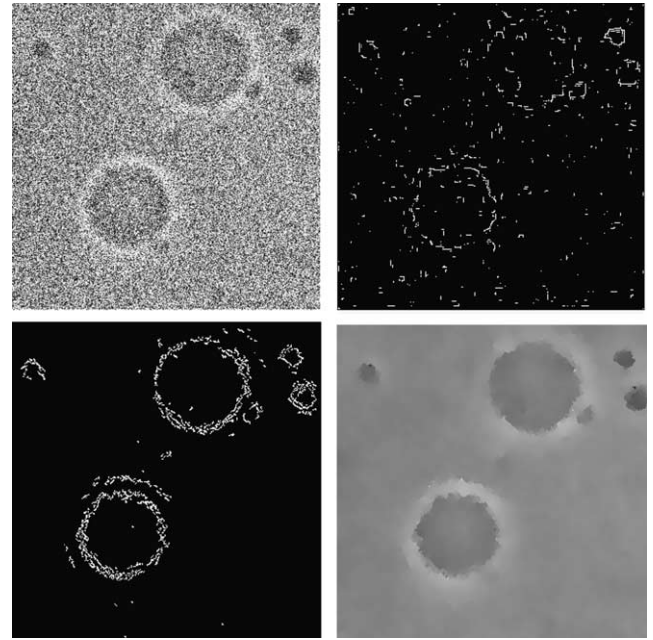

Fig. 6. A noisy image of cells (top left) and its segmented image using *DroG* edge detector (top right) segmented and smoothed image using GI method with $\mu = 100$ (bottom left and right, respectively).

detector with two different threshold values. The other parameters are chosen empirically optimal. As can be seen from Fig. 5(b) and (c), if the threshold is chosen so that a closed contour is obtained for the object, noise is also segmented in some parts of the image as depicted in Fig. 5(c). If the threshold increases to remove the 'segmented noise', then according to Fig. 5(d), the segmentation does not result in a close contour as expected. The GI algorithm is also applied to the noisy image of Fig. 5(b), and the segmented image includes a closed contour with virtually not segmented noise as depicted in Fig. 5(e). This clearly indicates a better performance for the GI algorithm compared to the *DroG* edge detector.

For comparison, the proposed GI algorithm in this paper and a *DroG* based edge detector have been applied to a real world image, a noisy image of polymersomes cells. As depicted in Fig. 6, *DroG* edge detector using empirically optimised parameters partially segment the objects and fail to avoid detecting noise. However, better segmentation result is achieved by using the GI algorithm. The smoothed image is calculated with $\mu = 100$. GI algorithm has also been applied to Lena, Cameraman, and Golden gate images contaminated with Gaussian noise with SNR=10.25, 5.81 and 8.25, respectively. Segmentation and smoothing are achieved by $\mu = 5$ as shown in Figs. 7–9.

5. Conclusion

A nonlinear functional is introduced in this paper for segmentation and noise reduction of images. The proposed functional is less complex than the Mumford–Shah functional, and its implementation is consequently numerically more efficient. A noniterative method based on intrinsic properties of

Fig. 7. Lena image (top left) and its noisy image contaminated with the Gaussian noise with SNR=10.25 (top right) segmented and smoothed images using the GI method with $\mu=5$ (bottom left and right, respectively).

a differentiable surface approximating the original image is proposed. Results indicate that this method is very robust in the presence of noise and more effective than methods based on *DroG* such as the Canny operator. The proposed method is generic and can be applied to signals and 3D images for segmentation and noise reduction.
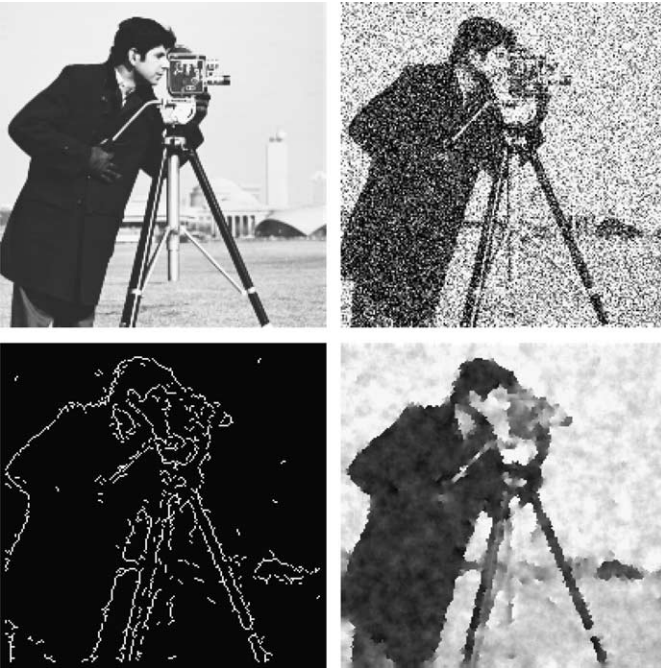

Fig. 8. Cameraman image (top left) and its noisy image contaminated with the Gaussian noise with SNR=5.81 (top right) segmented and smoothed images using the GI method with $\mu=5$ (bottom left and right, respectively).

Fig. 9. Golden gate image (top left) and its noisy image contaminated with the Gaussian noise with SNR=8.25 (top right) segmented and smoothed images using the GI method with $\mu=5$ (bottom left and right, respectively).

Appendix

In this appendix, we calculate metric and curvature tensor by assuming that the differentiable surface is a Monge patch $\mathbf{S}$. Normal unit vector $\mathbf{N}$, b_{ij} and g_{ij} are calculated as [11,12]:

$$g_{11} = \partial_1\mathbf{S}\cdot\partial_1\mathbf{S} = (\mathbf{e}_1 + f_{;1}\mathbf{e}_3)\cdot(\mathbf{e}_1 + f_{;1}\mathbf{e}_3) = 1 + f_{;1}^2$$

$$g_{12} = \partial_1\mathbf{S}\cdot\partial_2\mathbf{S} = (\mathbf{e}_1 + f_{;1}\mathbf{e}_3)\cdot(\mathbf{e}_2 + f_{;2}\mathbf{e}_3) = f_{;1}f_{;2}$$

$$g_{22} = \partial_2\mathbf{S}\cdot\partial_2\mathbf{S} = (\mathbf{e}_2 + f_{;2}\mathbf{e}_3)\cdot(\mathbf{e}_2 + f_{;2}\mathbf{e}_3) = 1 + f_{;2}^2$$

$$\mathbf{N} = \frac{\partial_1\mathbf{S}\times\partial_2\mathbf{S}}{|\partial_1\mathbf{S}\times\partial_2\mathbf{S}|} = \frac{-f_{;1}\mathbf{e}_1 - f_{;2}\mathbf{e}_2 + \mathbf{e}_3}{\sqrt{1 + f_{;1}^2 + f_{;2}^2}}$$

$$b_{11} = \partial_1^2\mathbf{S}\cdot\mathbf{N} = \frac{f_{;11}}{\sqrt{1 + f_{;1}^2 + f_{;2}^2}}$$

$$b_{12} = \partial_1\partial_2\mathbf{S}\cdot\mathbf{N} = \frac{f_{;12}}{\sqrt{1 + f_{;1}^2 + f_{;2}^2}}$$

$$b_{22} = \partial_2^2\mathbf{S}\cdot\mathbf{N} = \frac{f_{;22}}{\sqrt{1 + f_{;1}^2 + f_{;2}^2}}$$

where $f_{;i} = \partial f/\partial x^i$ and $f_{;ij} = \partial^2 f/\partial x^j\partial x^i$. Riemann curvature tensor and discriminant of metric tensor can therefore be rewritten as

$$\Re = b_{12}^2 - b_{11}b_{22} = \frac{f_{;12}^2 - f_{;11}f_{;22}}{1 + f_{;1}^2 + f_{;2}^2}$$

$$g = \sqrt{g_{11}g_{22} - g_{12}^2} = \sqrt{1 + f_{;1}^2 + f_{;2}^2}$$

To find the points in $x^1 x^2$ plane where g is maximum, the zero-crossing in the directional derivative along unit vector normal to contour, i.e. $\partial g / \partial n$ is examined. To ensure that in edge candidate points, g is maximised, $\partial^2 g / \partial n^2$ should be negative. This can be written as:

$$\frac{\partial g}{\partial n} = \vec{\nabla} g \cdot \mathbf{n} = (g_{;1}\mathbf{e}_1 + g_{;2}\mathbf{e}_2)$$
$$\cdot \left(\frac{g_{;1}}{\sqrt{g_{;1}^2 + g_{;2}^2}} \mathbf{e}_1 + \frac{g_{;2}}{\sqrt{g_{;1}^2 + g_{;2}^2}} \mathbf{e}_2 \right) = \sqrt{g_{;1}^2 + g_{;2}^2}$$

$$\frac{\partial^2 g}{\partial n^2} = \frac{\partial}{\partial n}\left(\frac{\partial g}{\partial n}\right) = \vec{\nabla}\left(\frac{\partial g}{\partial n}\right) \cdot \mathbf{n}$$
$$= \left(\frac{g_{;1}g_{;11} + g_{;2}g_{;12}}{\sqrt{g_{;1}^2 + g_{;2}^2}} \mathbf{e}_1 + \frac{g_{;1}g_{;12} + g_{;2}g_{;22}}{\sqrt{g_{;1}^2 + g_{;2}^2}} \mathbf{e}_2 \right)$$
$$\cdot \left(\frac{g_{;1}}{\sqrt{g_{;1}^2 + g_{;2}^2}} \mathbf{e}_1 + \frac{g_{;2}}{\sqrt{g_{;1}^2 + g_{;2}^2}} \mathbf{e}_2 \right)$$

Therefore, in edge points the following inequality should apply

$$\frac{\partial^2 g}{\partial n^2} = \frac{g_{;1}^2 g_{;11} + 2g_{;1}g_{;2}g_{;12} + g_{;2}^2 g_{;22}}{g_{;1}^2 + g_{;2}^2} < 0$$

References

[1] M. Kass, A. Witkin, D. Terzopoulos, Snakes: active contour models, Int. J. Comput. Vis. 1 (1987) 321–331.

[2] D. Mumford, J. Shah, Optimal approximations by piecewise smooth functions and associated variational problems, Commun. Pure Appl. Math. 42 (4) (1989) 577–688.

[3] J.M. Morel, S. Solimini, Variational Methods in Image Segmentation with Seven Image Processing Experiments, Birkhauser, Boston, 1995.

[4] G. Aubert, P. Kornprobst, Mathematical Problems in Image Processing: Partial Differential Equations and the Calculus of Variations, Springer, New York, 2002.

[5] A. Tsai, A. Yezzi, A.S. Willsky, Curve evolution implementation of the Mumford–Shah functional for image segmentation, denoising, interpolation and magnification, IEEE Trans. Image Process. 10 (8) (2001) 1169–1186.

[6] T.F. Chan, L.A. Vese, Active contours without edges, IEEE Trans. Image Process. 10 (2) (2001) 266–277.

[7] M. Hintermuller, W. Ring, An inexact-CG-type active contour approach for the minimization of the Mumford–Shah functional, J. Math. Imaging Vis. 20 (2004) 19–42.

[8] J.A. Sethian, Levet Set Methods: Evolving Interfaces in Geometry, Fluid Mechanics, Computer Vision and Material Science, Cambridge University Press, Cambridge, 1996.

[9] U.B. Manderscheid, Introduction to the Calculus of Variations, Chapman & Hall, London, 1991.

[10] I.M. Gelfand, S.V. Fomin, Calculus of Variations, Prentice-Hall, New Jersey, 1963.

[11] M.M. Lipschutz, Theory and Problems of Differential Geometry, Schaum's Outline Series, McGraw-Hill, New York, 1969.

[12] M.P. Carmo, Differential Geometry of Curves and Surfaces, Prentice-Hall, New Jersy, 1976.

[13] J. Canny, A computational approach to edge detection, IEEE Trans. Pattern Anal. Mach. Intell. 8 (6) (1986) 679–698.

[14] E. Kreyszig, Advanced Engineering Mathematics, Wiley, London, 1999.

[15] V. Caselle, R. Kimmel, G. Sapiro, Geodesic active contours, Procedings of the Fifth International Conference on Computer Vision, IEEE Computer Society Press, Silverspring, MD, 1995, pp. 694–699.

[16] V. Caselles, R. Kimmel, G. Saprio, Geodesic active contours, Int. J. Comput. Vis. 22 (1) (1997) 61–79.

[17] L.A. Vese, T.F. Chan, A multiphase level set framework for image segmentation using the Mumford and Shah model, Int. J. Comput. Vis. 50 (3) (2002) 271–293.

[18] T.F. Chan, B.Y. Sandberg, L.A. Vese, Active contours without edges for vector-valued images, J. Vis. Commun. Image Rep. 11 (2000) 130–141.

[19] T.F. Chan, L.A. Vese, Level set algorithm for minimising the Mumford–Shah functional in image processing, Proceedings of the IEEE Workshop on Variational and Level Set Methods in Computer Vision, 2001, pp. 161–168.

[20] L.A. Vese, Multiphase object detection and image segmentation, in: S. Osher, N. Paragios (Eds.), Geometrical Level Set Methods in Imaging, Vision, and Graphics, Springer, New York, 2003, pp. 175–194.

[21] A.N. Tikhonov, V.Y. Arsenin, Solutions of Ill-posed Problems, Winston & Sons, Washington, DC, 1977.

[22] L. Rudin, S. Osher, E. Fatemi, Nonlinear total variation based noise removal algorithms, Physica D 60 (1992) 259–268.

[23] W. Hinterberger, M. Hintermuller, K. Kunisch, M. von Oehsen, O. Scherzer, Tube methods for BV regularization, J. Math. Imaging Vis. 19 (2003) 219–235.

[24] S. Mahmoodi, B.S. Sharif, Noise reduction, smoothing, and time interval segmentation of noisy signals using an energy optimisation method, IEE Proceedings Vision, Image and Signal Processing, in press.

[25] S. Mahmoodi, B.S. Sharif, Signal segmentation and denoising algorithm based on energy optimisation, Signal Process. 85 (2005) 1845–1851.

[26] D.C. Kay, Tensor Calculus, Schaum's Outline Series, McGraw-Hill, New York, 1988.